Distribution of the color fields around static quarks: Lattice sum rules

Richard W. Haymaker
Department of Physics and Astronomy, Louisiana State University, Baton Rouge, Louisiana 70803

J. Wosiek
Chair of Computer Science, Jagellonian University, Institute of Physics, Reymonta 4, Cracow, Poland
(Received 6 November 1990)

A lattice Monte Carlo study of the color fields in the sector of static $q\bar{q}$ pairs is reported. Lattice sum rules relating these observables to the $q\bar{q}$ potential are tested in detail. As a by-product the β function of the SU(2) Yang-Mills theory is determined with high accuracy.

I. INTRODUCTION

For many years lattice gauge techniques have provided a simple and appealing picture of confinement based on flux-tube formation around color charges. The early simulations concentrated on global quantities such as the vacuum energy in the presence of the static sources which gives the heavy-quark potential. Improved numerical techniques and computing power allow now a study of local quantities, i.e., chromoelectric and chromomagnetic flux, in considerable detail. These studies are closely related. The work required to pull a quark-antiquark pair apart to a distance R, as measured by the potential $V(R)$, must show up in the form of chromoenergy density. Hence a physical constraint on these studies is in the form of a sum rule which states that the sum of this energy density over all space must in turn give the potential back.

The flux problem on the lattice was first studied in 1983 by Fukugita and Niuya,[1] and later by Flower and Otto[2] and Sommer.[3,4] Michael and co-workers have made extensive studies of the pure gauge sector.[5–10] In a series of papers Markum and co-workers have studied a number of aspects of the heavy-quark problem, including the chiral condensate and the quark-polarization effects.[11–13] de Forcrand, Linke, and Stamatescu have also studied the breakup of the string caused by dynamical fermions.[14] Caldi and Sterling[15] obtained precise results in $2+1$ dimensions. Campostrini *et al.*[16] and Duncan and Mawhinney[17] saw that by cooling the configurations some features of the flux tube survive when quantum fluctuations are artificially suppressed, attributing the features to classical configurations. The quality of current simulations may soon allow for a quantitative test of various analytical models of the confining tube. The seminal work on this problem goes back to the paper of Nielsen and Olesen who have first found the vortex solution of the Abelian Higgs model.[18] In another fundamental approach, Lüscher, Münster, and Weisz have studied the bosonic string model of the effective tube.[19,20] Baker, Ball, and Zachariasen have obtained the explicit solution of the effective dual formulation of the Yang-Mills theory.[21] Also, recently, Bagan has proposed a model of the chromoelectric flux tube which is inspired by the Shifman-Vainshtein-Zakharov (SVZ) sum rules.[22]

Our study of the flux started in 1987 when we first obtained the distribution of the $E_{\parallel}$ component for large $q\bar{q}$ distances.[23–28] In the present simulations we measure rather precisely the complete energy and action distributions. These data are then extrapolated to the infinite-time extent of the Wilson loop in order to minimize the effect of the creation and annihilation of static quarks. The techniques employed to get high-precision flux data also gave accurate Wilson loops, i.e., the potential. Therefore, we are able to give the first direct test of the Michael sum rules relating the potential to the sum over energy density.[5] This is done in this article. In a separate paper we look in detail at the spatial behavior of the flux.[28]

II. SIMULATION

The computations were done on the FPS AP264 array processor at LSU. Our lattice size was a $17^3 \times 20$ hypercube with helical boundary conditions. Updating was done checkerboard fashion, which requires space dimensions odd and the time dimensions even. For SU(2) overrelaxation is microcanonical, and hence the Metropolis method is needed to sample configurations with different energies and/or actions; hence, we alternated the two-hit Metropolis method with overrelaxation,[29] which gave a good sweep-to-sweep decorrelation. We measured after each five sweeps and grouped our data into bins of five measurements each. We ran at three values of β: 2.3, 2.4, and 2.5.

A. Wilson loops

We introduce static sources via $R \times T$ Wilson loops. Quantum mechanically, the Wilson loop provides the projection onto the $q\bar{q}$ sector of the Hilbert space. Projection onto the ground state of the $q\bar{q}$ state is obtained only when the time extent of the loop tends to infinity. On the other hand, the interest lies in the shape of the flux tube for large *space* separations. However, the large space and time separations are very difficult to achieve simultaneously because of the exponential suppression of

the signal with the area of the loop. For that reason the straightforward measurement of these quantities would lead to prohibitive computer time or intolerable errors.

A very effective way to reduce fluctuations in these quantities is to do as many integrations analytically as is practical. This is the analytic version of the multihit procedure proposed by Parisi, Petronzio, and Rapuano.[30] For example, the one-link integral can be evaluated using

$$\int [dU]Ue^{(\beta/2)\mathrm{tr}(UK^\dagger)}=\frac{I_2(\beta b)}{I_1(\beta b)}V\int [dU]e^{(\beta/2)\mathrm{tr}(UK^\dagger)}\ , \tag{1}$$

where K is the sum of six "staples" coupling to a given U in the action,[30] and $I_n(x)$ is the modified Bessel function. The sum of SU(2) matrices in the $j=\frac{1}{2}$ representation is a multiple of an SU(2) matrix which we denote by V:

$$K=bV,\quad b\equiv(\det K)^{1/2}\ . \tag{2}$$

The effect of Eq. (1) when applied to a simulation is to replace a link U occurring in the Wilson loop by a corresponding sum of "staples" V. This is indicated in Fig. 1. Since K involves 18 links, one can expect the fluctuations of the ensemble of K's to be suppressed compared to a single link U in each measurement. As one goes to larger values of β, the corresponding correlation length increases and there is less cancellation of fluctuations over the 18-link structure. We indeed find the suppression more effective for smaller values of β.

This result is useful as long as subsequent analytic integrations do not involve one of the links in K. For example, this will work for those links that make up the sides of a Wilson loop of size 2×2, or larger, as long as one link at each corner is left in its original form. Analytic treatment of all links was done by generalizing Eq. (1) to more complicated structures. The cases of four links in a plaquette and two links that form corners have been derived by Bunk.[31] Figure 1 shows which staples are relevent in the analytic integrations. These two cases cannot be given in closed form, but can be expressed by a rapidly convergent character expansion.[25]

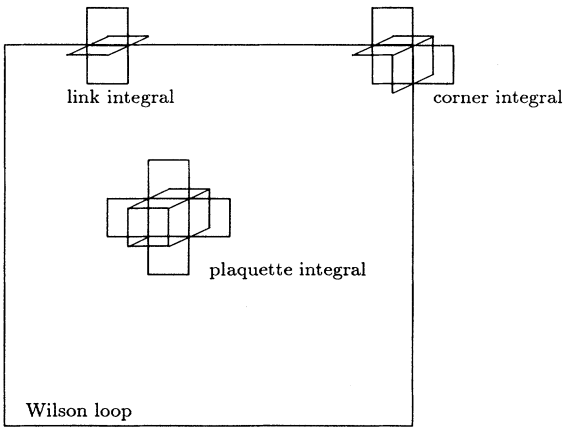

FIG. 1. Links involved in link, corner, and plaquette integrals.

We measured most rectangular loop sizes $R\times T$ from 1×1 to 6×9 and, in one case, $R=7$, as shown in Table I. The $1\times T$ loops have notably larger errors than, for example, $2\times T$ loops. This is because the analytic methods to suppress the fluctuations were not employed for the $1\times T$ case.

B. Flux

The lattice observable needed to measure the flux is[1-4,23-28]

$$f^{\mu\nu}(x)=\frac{\beta}{a^4}\left[\frac{\langle WP_x^{\mu\nu}\rangle}{\langle W\rangle}-\langle P\rangle\right] \tag{3}$$

$$\approx\frac{\beta}{a^4}\left[\frac{\langle WP_x^{\mu\nu}-WP_{x_R}^{\mu\nu}\rangle}{\langle W\rangle}\right]\ , \tag{4}$$

where W is the Wilson loop, $P_x^{\mu\nu}$ is the plaquette located at x, and a is the lattice spacing. In the classical continuum limit

$$f^{\mu\nu}\overset{a\to 0}{\to}-\frac{1}{2}\langle(F^{\mu\nu})^2\rangle_{q\bar{q}-\mathrm{vac}}\ , \tag{5}$$

where the notation $\langle\cdots\rangle_{q\bar{q}-\mathrm{vac}}$ means the difference of the average values in the $q\bar{q}$ and vacuum state. From now on we shall be using field components in Minkowski space and hence

$$f^{\mu\nu}\to\tfrac{1}{2}(-B_1^2,-B_2^2,-B_3^2;E_1^2,E_2^2,E_3^2)\ . \tag{6}$$

Correspondence between various components and $f^{\mu\nu}$ is standard: Space-space plaquettes are magnetic, and space-time plaquettes are electric. The energy and action densities are, respectively,

$$\epsilon=\tfrac{1}{2}(E^2+B^2)\ , \tag{7}$$

$$\gamma=\tfrac{1}{2}(E^2-B^2)\ . \tag{8}$$

Since, however, the magnetic contribution turns out to be negative, there is a strong cancellation between the two terms in the energy, while they are enhanced in the action.

Because of the large amount of data generated and because of the difficulty of getting good statistics, the data were folded on rectangular symmetry planes. We also limited the measured flux to a fiducial volume consisting of a closed volume surrounding the Wilson-loop four lattice spacings in every direction. We measured all six components of the flux.

Some enhancements in the signal to noise is vital to measure the flux. In addition to the Wilson-loop analytic integrations, another enhancement is almost trivial, but contributed significantly in reducing errors.[23] That is indicated in Eq. (4) in which the flux is measured relative to a distant reference point x_R. This does not change the lattice average, but the main fluctuations of PW, which are due to the Wilson loop itself, cancel when the difference [Eq. (4)] is computed configuration by configuration. By taking for x_R a point where the correlation vanishes, the two forms in Eq. (3,4) are equal. In practice, we take for x_R a corner of the hypercubic fidu-

TABLE I. Wilson loops, (a) $\beta=2.3.*$, 195 meas; †, 240 meas. (b) $\beta=2.4.*$, 200 meas; †, 540 meas; ‡, 230 meas; ○, 140 meas. (c) $\beta=2.5.*$, 180 meas; †, 200 meas; ‡, 210 meas.

R \ T	1	2	3	4	5	6	7	8	9
					(a)				
1	0.602 421* 0.000 036								
2		0.180 240* 0.000 054	0.088 931* 0.000 049	0.044 600* 0.000 039	0.022 473* 0.000 028	0.011 343* 0.000 019	0.005 729* 0.000 012	0.002 895* 0.000 008	0.001 420† 0.000 005
3			0.035 334* 0.000 038	0.014 564* 0.000 026	0.006 082* 0.000 017	0.002 552* 0.000 011	0.001 077* 0.000 007	0.000 454* 0.000 005	0.000 179† 0.000 002
4				0.005 046* 0.000 017	0.001 784* 0.000 010	0.000 634* 0.000 007	0.000 229* 0.000 004	0.000 083* 0.000 003	0.000 029† 0.000 002
5					0.000 535* 0.000 006	0.000 162* 0.000 004	0.000 050* 0.000 002	0.000 016* 0.000 002	0.000 004† 0.000 001
6						0.000 043* 0.000 002	0.000 013* 0.000 002	0.000 002† 0.000 001	
					(b)				
1	0.630 044† 0.000 016	0.424 987* 0.000 074	0.291 168* 0.000 089	0.200 229* 0.000 096	0.137 838* 0.000 102	0.094 917* 0.000 106	0.065 296* 0.000 107	0.044 902* 0.000 107	0.030 941* 0.000 107
2		0.222 554† 0.000 029	0.123 709† 0.000 030	0.069 973† 0.000 026	0.039 794† 0.000 020	0.022 672† 0.000 015	0.012 925† 0.000 011	0.007 370† 0.000 008	0.004 101‡ 0.000 076
3			0.059 244† 0.000 027	0.029 456† 0.000 021	0.014 829† 0.000 015	0.007 499† 0.000 011	0.003 799† 0.000 007	0.001 927† 0.000 005	0.000 958○ 0.000 007
4				0.013 170† 0.000 016	0.006 011† 0.000 011	0.002 766† 0.000 007	0.001 277† 0.000 005	0.000 592† 0.000 003	0.000 271○ 0.000 004
5					0.002 511† 0.000 007	0.001 062† 0.000 005	0.000 452† 0.000 003	0.000 194† 0.000 002	0.000 083○ 0.000 003
6						0.000 417† 0.000 003	0.000 165† 0.000 002	0.000 063○ 0.000 002	0.000 027○ 0.000 002
7							0.005 608○ 0.000 002	0.000 019○ 0.000 002	0.000 007○ 0.000 001
					(c)				
1	0.651 998† 0.000 022	0.456 541* 0.000 074	0.324 792* 0.000 091	0.231 935* 0.000 100	0.165 751* 0.000 107	0.118 494* 0.000 112	0.084 762* 0.000 114	0.060 682* 0.000 114	0.043 368* 0.000 114
2		0.258 078† 0.000 045	0.154 985† 0.000 049	0.094 714† 0.000 045	0.058 205† 0.000 038	0.035 836† 0.000 031	0.022 081† 0.000 024	0.013 609† 0.000 018	0.008 389† 0.000 014
3		0.154 839‡ 0.000 048	0.083 249† 0.000 049	0.046 378† 0.000 043	0.026 160† 0.000 034	0.014 823† 0.000 026	0.008 418† 0.000 019	0.004 784† 0.000 013	0.002 722† 0.000 009
4		0.094 577‡ 0.000 045	0.046 375† 0.000 043	0.024 055† 0.000 036	0.012 730† 0.000 027	0.006 794† 0.000 020	0.003 643† 0.000 014	0.001 957† 0.000 010	0.001 053† 0.000 006
5		0.058 085‡ 0.000 038	0.026 051‡ 0.000 033	0.012 644‡ 0.000 025	0.006 311‡ 0.000 018	0.003 184‡ 0.000 013	0.001 615‡ 0.000 009	0.000 849† 0.000 006	0.000 436† 0.000 004
6		0.035 737‡ 0.000 030	0.014 741‡ 0.000 025	0.006 726‡ 0.000 018	0.003 183‡ 0.000 013	0.001 525‡ 0.000 009	0.000 739‡ 0.000 006	0.000 357‡ 0.000 004	0.000 172‡ 0.000 003
7		0.022 006‡ 0.000 023	0.008 355‡ 0.000 018	0.003 588‡ 0.000 013	0.001 614‡ 0.000 009	0.000 737‡ 0.000 006	0.000 343‡ 0.000 004	0.000 159‡ 0.000 003	

cial volume as the "point at infinity."

In the vectorized code, we save the long vectors of Wilson loops (or fat Wilson loops) corresponding to all locations of the loop and similarly for all locations and orientations of the plaquette. We then calculate the cross correlation between these two long vectors. To do a naive correlation measurement, an estimate of computer time t gives

$$t \propto V_{\text{lattice}} \times V_{\text{fiducial}} , \tag{9}$$

whereas if one employs fast Fourier transforms, we obtain

$$t \propto V_{\text{lattice}} \times \log_2(V_{\text{lattice}}) . \tag{10}$$

Given the size of our fiducial volume, the fast Fourier transform was essential to beat down computer time.

The fast Fourier transforms give all the correlations, not just those in the fiducial volume. However, when the fat operators indicated in Fig. 1 get too close together, the analytic expressions, derived for the case of nonoverlapping links, break down. Therefore, one must recalculate those correlations, dropping the analytic integrations as necessary. Plaquettes that share a link with Wilson-loop links had the least fluctuation suppression. We calculated plaquette correlations in all cases using the maximum number of analytic integrations allowed by the one-link, corner, and plaquette integrals mentioned above. This meant dropping one or two of the analytic one-link integrations when the plaquette touched the Wilson line.

III. POTENTIAL

The $q\bar{q}$ potential was extensively studied in the literature,[4,8,32,33] and the following discussion is intended to demonstrate the consistency of our new and more precise results with earlier works. Second, it is required for the completeness of the subsequent discussion of our local measurements of the energy density.

As usual, we obtain the energy of the static $q\bar{q}$ pair from the largest eigenvalue of the lattice transfer matrix projected onto the $q\bar{q}$ sector of the Hilbert space. To this end one fits the time dependence of the average value of the Wilson loop $W(R,T)$ to the expression

$$\langle W(R,T)\rangle = \sum_i R_i e^{-E_i(R)T} , \tag{11}$$

where $R_i = |\langle 0|\hat{S}|i\rangle|^2$ characterizes the ability of the operator $\hat{S}$ (here the spacelike string of $\hat{U}$'s) to excite the state $|i\rangle$. To extract reliability the ground-state energy $E_0(R)$, one needs the large-T limit of $\langle W(R,T)\rangle$. With a shorter T interval available, more excited states contribute to the sum. To get an idea of how important various contributions are, and how far we are from the $T=\infty$ limit, we rewrite Eq. (11):

$$-\frac{1}{T}\ln\langle W(R,T)\rangle = E_0 - \frac{1}{T}C(T) , \tag{12}$$

with

$$C(T) = \ln\left[R_0 + \sum_{i\geq 1} R_i e^{-T[E_i(R)-E_0(R)]}\right] . \tag{13}$$

For large T, $C(T)$ is independent of T; hence plotting the left-hand side (LHS) of Eq. (12) vs $1/T$ would show directly how important are higher states and how big is the required extrapolation. Figure 2 shows such a graph. Indeed, the $1/T$ dependence is almost linear and higher states show up only for largest $1/T$. As expected, for larger R the asymptotic linear regime starts at smaller $1/T$ values. The extrapolated intercept values agree well with the "time-dependent" estimates of the energies

$$aE^{\text{es}}(R) = \ln[\langle W(R,T)\rangle / \langle W(R,T+1)\rangle] .$$

Table II summarizes the results of fitting $\langle W(R,T)\rangle$ with the expression Eq. (11). Two or three states were used, and the $T_{\min}$ was also varied to check the stability. Errors on the parameters are standard MINUIT errors; i.e., they correspond to the change of χ^2 by 1. They should be regarded with some caution since no correlations between Monte Carlo data points were included. Both E_0 and E_1 are stable under the variation of $T_{\min}$ and the number of states used in the fit. Resulting values agree rather well with other authors.[4,10,33]

In order to push for larger distance, we have also fitted our loops for $R = 7a$–$9a$, interpreting the shorter dimensions as a time. This brings us to probing $q\bar{q}$ distances ~ 1.5 fm. However, in this case the T interval available for fitting is reduced and the values of the slopes E_i are consistently overestimated due to the influence of excited states. This explains the deviation of the rightmost points from the common curves shown in Figs. 3 and 4.

To check for scaling, we merely plotted $E_0(R)$ in physical units for all three β values [cf. Fig. 3(a)]. In transforming from lattice to physical units, we used the values of the running lattice constant $a(\beta)$ quoted in Refs. 4

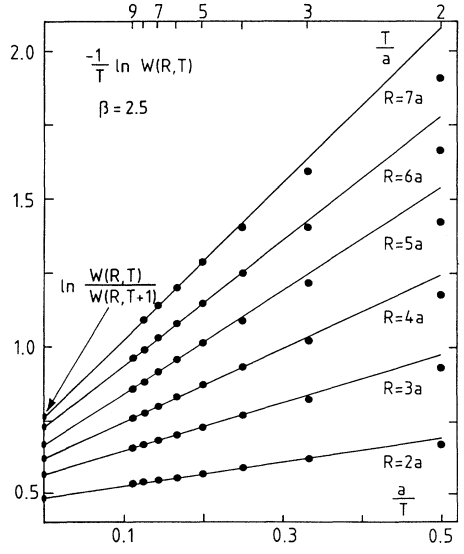

FIG. 2. Testing domination of the lowest state for $\langle W(R,T)\rangle$.

and 10; cf. Table III. [Since our $E_0(R)$ agrees so well with Sommer's on axis potential, we would have obtained the same values for $a(\beta)$ had we repeated the analysis of Sommer or Michael.] It is evident from Fig. 3(a) that our lattice string tension scales in accordance with the $a(\beta)$ quoted in Table III. Another confirmation of the consistency comes from the values of the self-energy. The ground-state energy of the static $q\bar{q}$ pair is conveniently parametrized by

$$E_0(R)=\frac{\alpha}{R}+\sigma R+\frac{c(\beta)}{a(\beta)}\ , \tag{14}$$

where c/a is the ultraviolet-divergent self-energy of the pointlike sources. This term prevents $E_0(R)$ from scaling. However, the *shape* of the R dependence remains the same for all β. This is readily seen from Fig. 3(a). From the amount of the shift required to bring the three curves together [Fig. 3(b)], we get, for the corresponding

TABLE II. Results of the fits of the time dependence of the Wilson loops.

β	R	R_0	E_0	R_1	E_1	N_s	$T_{\min}-T_{\max}$	$\chi^2/N_{\rm DF}$
				(a)				
2.3	2	0.6818(06)	0.6827(03)	0.2147(27)	1.799(02)	3	2–8	0.030/1
		0.6806(35)	0.6825(09)	0.168(76)	1.68(16)	2	3–8	0.012/2
		0.6820(21)	0.6828(06)	0.243(27)	1.838(73)	2	2–8	0.037/3
	3	0.4562(14)	0.8645(07)	0.3354(52)	1.873(04)	3	2–8	0.074/1
		0.4508(95)	0.8629(34)	0.229(40)	1.685(92)	2	3–8	0.012/2
		0.4563(45)	0.8645(18)	0.340(33)	1.877(73)	2	2–8	0.076/3
	4	0.3019(18)	1.027(02)	0.3971(78)	2.104(06)	3	2–8	0.321/1
		0.2849(67)	1.020(02)	0.179(66)	1.67(19)	2	3–8	0.139/2
		0.3020(53)	1.027(03)	0.400(44)	2.107(80)	2	2–8	0.323/3
	5	0.2061(19)	1.192(03)	0.3960(99)	2.400(76)	3	2–8	0.125/1
		0.192(17)	1.182(18)	0.15(12)	1.89(15)	2	3–8	0.051/2
		0.2065(55)	1.192(06)	0.449(62)	2.437(88)	2	2–8	0.061/1
	6	0.123(29)	1.328(42)	0.27(12)	2.31(48)	3	2–8	0.277/1
		0.1153(47)	1.319(09)	0.183(19)	2.086(19)	2	3–8	0.209/2
		0.1231(73)	1.328(14)	0.282(50)	2.32(11)	2	2–8	0.279/3
	7	0.0844(89)	1.487(28)	0.286(60)	2.66(10)	2	2–6	0.194/1
	8	0.067(23)	1.68(11)	0.61(14)	3.51(12)	2	2–6	0.055/1
				(b)				
2.4	1	0.8910(04)	0.3733(01)	0.1168(13)	1.892(01)	2	2–7	0.195/2
	2	0.6589(02)	0.5617(01)	0.2016(10)	1.637(01)	3	2–9	1.79/2
		0.6587(04)	0.5616(01)	0.2077(16)	1.636(01)	2	3–8	0.002/2
		0.6594(11)	0.5618(03)	0.255(18)	1.721(48)	2	2–8	0.047/3
	3	0.4421(15)	0.6796(06)	0.373(23)	1.800(03)	3	2–9	0.615/2
		0.4397(22)	0.6788(08)	0.271(52)	1.659(80)	2	3–8	0.034/2
		0.4418(17)	0.6795(06)	0.362(21)	1.785(41)	2	2–8	0.218/3
	4	0.2791(06)	0.7698(05)	0.2480(21)	1.655(02)	3	2–9	1.02/2
		0.2789(28)	0.7697(16)	0.245(39)	1.649(71)	2	3–8	0.092/2
		0.2835(19)	0.7719(12)	0.385(21)	1.855(40)	2	2–8	0.610/3
	5	0.1712(07)	0.8486(08)	0.2078(20)	1.666(02)	3	2–9	0.442/2
		0.1713(31)	0.8486(28)	0.209(30)	1.668(66)	2	3–8	0.170/2
		0.1775(20)	0.8534(20)	0.352(19)	1.919(41)	2	2–8	0.856/3
	6	0.1004(06)	0.9168(13)	0.1702(18)	1.685(03)	3	2–9	1.51/2
		0.1083(21)	0.9275(35)	0.296(16)	1.973(44)	2	2–7	0.650/2
	7	0.0696(05)	1.010(02)	0.2670(26)	2.141(03)	2	2–7	2.91/2
	8	0.0484(13)	1.111(06)	0.283(23)	2.455(54)	2	2–7	1.66/2
	9	0.0260(25)	1.153(20)	0.176(37)	2.38(13)	2	2–7	0.822/2
				(c)				
2.5	1	0.8871(03)	0.3355(01)	0.0940(11)	1.716(01)	2	2–7	0.135/2
	2	0.6541(65)	0.4841(16)	0.249(98)	1.62(28)	2	2–7	0.028/2
	3	0.4411(19)	0.5656(08)	0.346(17)	1.653(37)	2	2–7	0.089/2
	4	0.2859(26)	0.6235(16)	0.361(24)	1.680(50)	2	2–7	0.274/2
	5	0.1906(22)	0.6822(20)	0.357(28)	1.814(55)	2	2–7	3.44/2
	6	0.1241(19)	0.7331(27)	0.324(27)	1.905(58)	2	2–7	4.20/2
	7	0.0797(16)	0.7800(37)	0.270(23)	1.962(60)	2	2–7	5.60/2
	8	0.0546(10)	0.8357(38)	0.337(41)	2.307(73)	2	2–7	5.07/2
	9	0.0375(08)	0.8949(50)	0.368(52)	2.577(83)	2	2–7	5.05/2

TABLE III. Running lattice constant $a(\beta)$.

β	$a(\beta)$
2.3	0.171 fm
2.4	0.128 fm
2.5	0.089 fm

differences of the self-energies,

$$\Delta(2.5,2.4)=0.38 \text{ GeV} \quad (0.36 \text{ GeV}) ,$$
$$\Delta(2.4,2.3)=0.18 \text{ GeV} \quad (0.20 \text{ GeV}) , \tag{15}$$

where $\Delta(\beta_1,\beta_2)=c(\beta_1)/a(\beta_1)-c(\beta_2)/a(\beta_2)$, which compare favorably with Sommer numbers quoted in parentheses.

Finally, our result for the energy of the first excited state of the gluon field in the $q\bar{q}$ sectors is shown in Fig. 4. Excited states were studied in detail by Perantonis, Huntley, and Michael[10] using combinations of the Monte Carlo and variational techniques. In contrast with E_0, the energy of the first excited state depends very weakly on the $q\bar{q}$ distance R. This was also seen in Ref. 10 and is reproduced by the bosonic string model. Our results agree with theirs to within 15% for $R \leq 6a$. Small systematic differences are probably due to our effective averaging over various representations of the discrete lattice symmetry group of the $q\bar{q}$ state. Again, at $R \geq 7a$, E_1 is overestimated because of too short a time extent of W available for fitting.

The energy of the first excited state E_1, more precisely the energy difference $\Delta_1=E_1-E_0$, controls the convergence of our flux measurements to their large-T limit and will play an important role in the flux analysis.

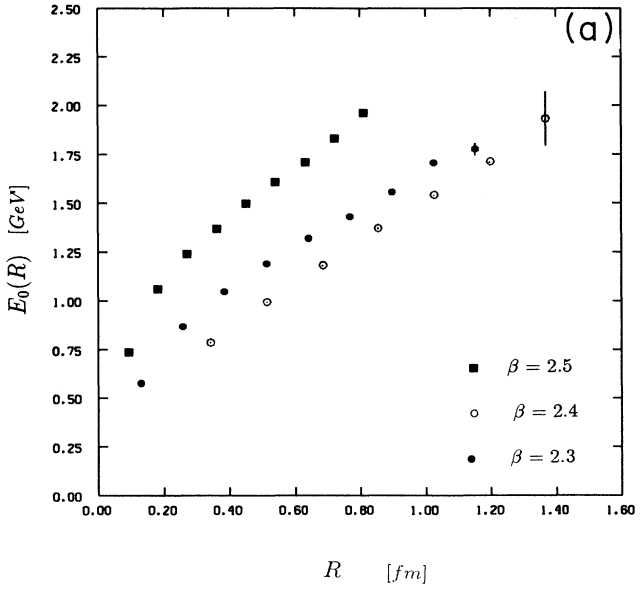

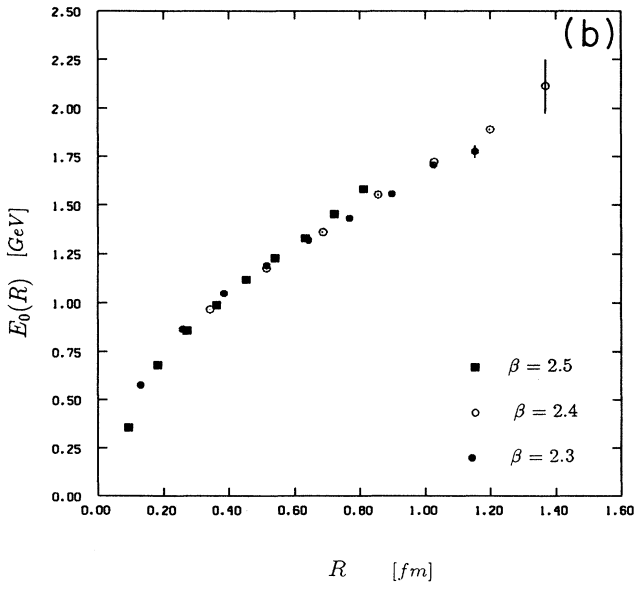

FIG. 3. Scaling of the ground-state energy of the static $q\bar{q}$ pair. (a) $E_0(R)$ in physical units for three values of β; (b) after shifts accounting for the differences of the self-energies.

IV. SUM RULES

A. Processing the data

Having established the consistency of our measurements with earlier data, we will describe shortly the procedure to compute the ground-state averages of the energy density and gluon condensate (also referred to as the action density). A more detailed discussion of this procedure can be found elsewhere.[28]

Since the geometrical centers of each of the six plaquettes, $P_{\mu\nu}(x)$, representing individual components of $f_{\mu\nu}$, are different, some interpolation procedure is needed before we can compute the energy or action densities. We do it in three steps. First, we project out the ir-

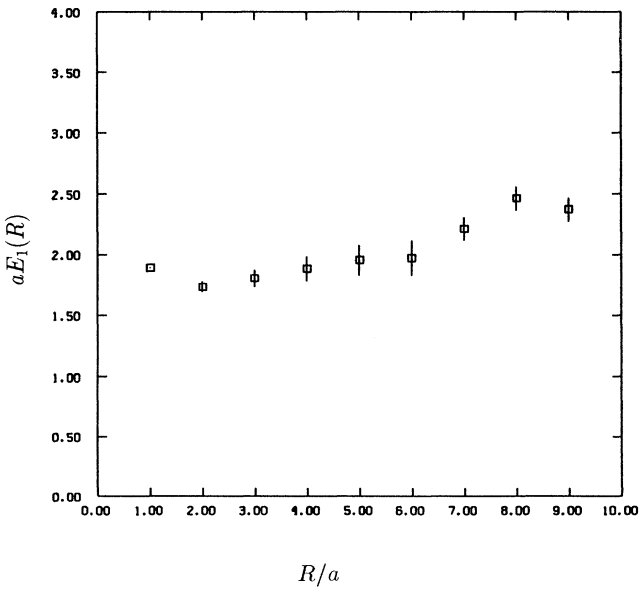

FIG. 4. Energy of the first excited state in the $q\bar{q}$ sector, $\beta=2.4$.

relevant dependence on the aximuthal angle ϕ (the $q\bar{q}$ axis is chosen to be the z direction). This gives us the four components $E_{\parallel}$, $E_{\perp}$, $B_{\perp}$, and $B_{\parallel}$ as a function of the transverse variable $x_{\perp}=(x^2+y^2)^{1/2}$ and z. Next, the value of any component at arbitrary $x_{\perp}$ is obtained by linear extrapolation, at fixed z, of the Monte Carlo data measured at adjacent $x_{\perp}$ points. Finally, the linear interpolation in z at fixed $x_{\perp}$ was performed to bring various components to the same longitudinal position. During the interpolation, errors were propagated linearly assuming the statistical independence of the measurements performed at different points. Global quantities like the total energy and the action were obtained by integrating numerically in $x_{\perp}$ and then adding contributions from different transverse slices. In spite of the apparent complications, the interpolation procedure averages out statistical fluctuations, and as a consequence, our final distributions are reasonably smooth and show rather small statistical errors. Only around the end points $x_{\perp}\sim 0$, $x_{\perp}\sim 5.5a$, where the interpolation turns into extrapolation, have we seen considerable buildup of the propagated errors. This is expected from standard error analysis.

The whole interpolation procedure was applied to our correlations [Eq. (4)] measured with the time-elongated Wilson loops $W(R,T)$, as well as to the $T=\infty$ space distributions which were obtained by fitting the T dependence of $f^{\mu\nu}(\mathbf{x},x_4=T/2;T,R)$ at each $\mathbf{x}$.[28] The difference between the two measures the contamination of the finite T data by the excited states.

B. Energy sum rule

The Michael sum rule for the energy reads[5]

$$\tfrac{1}{2}\sum_{\mathbf{x}}[E(\mathbf{x})^2+B(\mathbf{x})^2]=E_0(R)\ , \tag{16}$$

where both sides of Eq. (16) refer to the lowest quantum state of the Yang-Mills field in the sector of the Hilbert space, with the classical $q\bar{q}$ sources separated by the distance R. Two comments should be made before the detailed comparison.

(1) We have measured $f^{\mu\nu}$, and consequently ϵ, in the fiducial volume V_{fiducial} surrounding the sources by four lattice units in all directions. Beyond this distance the signal is (a) very small, (b) very noisy, and (c) bookkeeping much larger volume of observables is limited by the storage capacity of our machine. We also note that our procedure integrates effectively over the cylindrical volume of radius $x_{\perp}\leq 5.5a$ rather than summing the LHS of Eq. (16) in the rectangular box $x,y\leq 4a$.

(2) The success of the whole project of measuring the averages $f^{\mu\nu}(x)$ [Eq. (3)] is entirely dependent on the trick which replaces Eq. (3) with Eq. (4), where the difference of $WP^{\mu\nu}_{x}-WP^{\mu\nu}_{x_R}$, for some distant reference point x_R, is computed configuration by configuration instead of subtracting the averages.[23] For large enough x_R, the averages given both equations are equal, but fluctuations of the difference $WP^{\mu\nu}_{x}-WP^{\mu\nu}_{x_R}$ are much smaller (sometimes by two orders of magnitude), giving much smaller statistical errors of Eq. (4) compared to Eq. (3). This substantial reduction of noise was achieved at the price of giving up the exact normalization of our densities. The reference point x_R was chosen at the distance $(R/2+4,T/2+4,4,4)$ from the center of W, and for large Wilson loops, this separation was not enough to guarantee the proper (vacuum) normalization of our densities. In other words, precise measurement of the difference (4) detected small background values ϵ_B for $\epsilon(\mathbf{x})$ at large $x_{\perp}$ or z. Thus the detailed test of the sum rule must take into account the extensive contribution to the total energy $\Delta E=-V_{\text{fiducial}}\epsilon_B$.

Figure 5 clearly confirms the above considerations. It shows the energy contained in the cylindrical volume

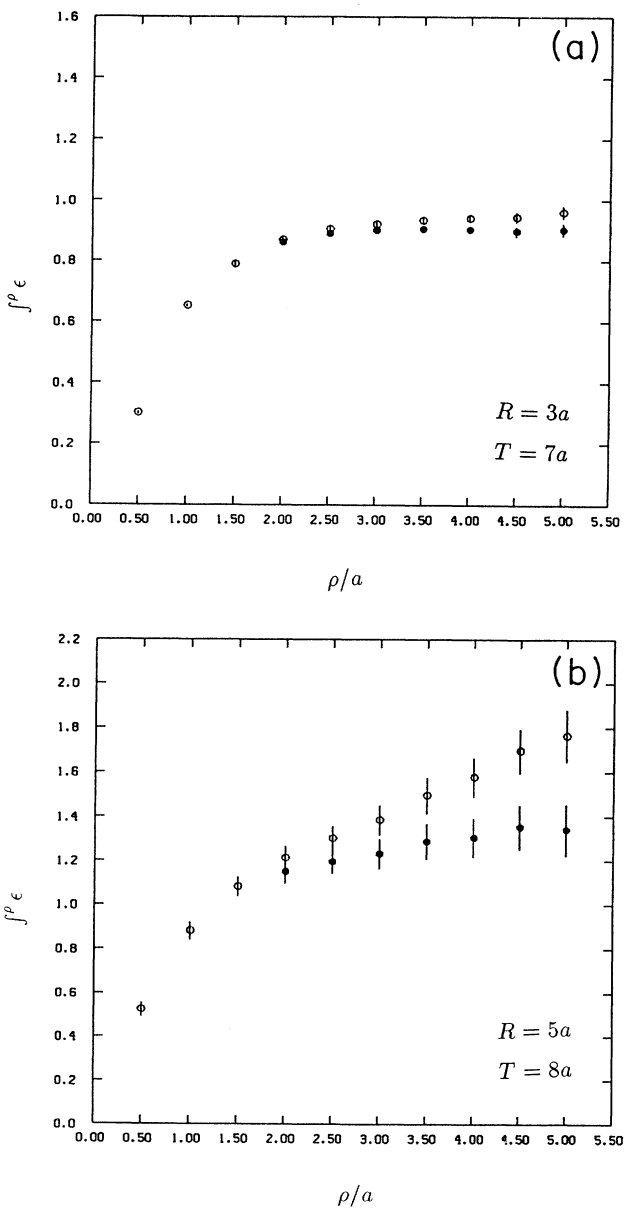

FIG. 5. Integrated, up to ρ, transverse profiles of the energy density (GeV). Open circles show uncorrected and solid circles show corrected cumulants; $\beta=2.4$.

with radius ρ and the length $R+8a$, as the function of ρ, for different $q\bar{q}$ distances R. For small $q\bar{q}$ separations ($R \leq 3$), the energy is contained in the first three units and the cumulative distribution saturates. For larger R's the transverse integration does not converge, giving the ρ-dependent cumulant. The value of ϵ_B can be extracted from this residual ρ dependence or, alternatively, read directly from the large-$x_\perp$ behavior of the density. Corrected cumulants are also shown. They are nicely constant, demonstrating the consistency of the subtraction procedure.

Finally, the test of the sum rule Eq. (16) is shown in Fig. 6. For small R, errors of the sum, though very small, are caused mainly by the uncertainties of the extrapolation and correction. For larger distance statistical fluctuations become equally important. Errors of the RHS of Eq. (16) are negligible. The agreement with the potential fits is satisfactory. Small ($\sim 10\%$) deviations at small R/a may result from the finite a effect, i.e., too large a grid for the precise description of the shape of the distribution around the small tubes.

C. Action sum rule

The action density $\gamma(x)$ is much easier to measure since it acquires positive contributions from all six components of $f^{\mu\nu}$; cf. Eq. (4). Consequently, the large-T extrapolation of the densities is much more reliable and less dependent on the choice of $T_{\min}$ and number of states used in the fit, also for the larger $q\bar{q}$ separations. This is clearly seen from Fig. 7, where the integrated transverse profile of the gluon condensate is shown. The upper band denotes the variation of the extrapolated (to $T=\infty$) values with the details of the fit (number of states and $T_{\min}$). Similarly, the background contribution is better controlled in this case. Corrected distribution is nicely saturating and depends rather weakly on the initial distribution, i.e., whether we start with the $T=7a, 8a$ or, extrapolated to $T=\infty$ data, we end up within the lower band shown in Fig. 7.

Typically, the action density is larger by the factor 7–9 than the corresponding energy densities. This agrees well with the main enhancement factor $\beta d\ \ln a/d\beta \approx 7.7$ also quoted in Ref. 4. The same number is also seen when we compare the string tension and the condensate tension—the amount of action stored in the unit length of the middle section of the tube (cf. Table IV). The corresponding transverse sum rule can be obtained from the action sum rule (an overdot denotes $d/d\beta$)

$$A(R) \equiv \frac{1}{2}\sum_{\mathbf{x}} [E(\mathbf{x})^2 - B(\mathbf{x})^2]$$

$$= -\beta \frac{\dot{a}}{a}\left[E_0(R) - \frac{c(\beta)}{a}\right] - \beta \frac{\dot{c}(\beta)}{a}\ , \qquad (17)$$

by differentiation with respect to R. At sufficiently large $q\bar{q}$ distances, the Coulomb contribution to $E_0(R)$ can be neglected and we get

$$\sigma_A \equiv \frac{1}{2}\sum_{\mathbf{x}_\perp, z=0} [E(\mathbf{x})^2 - B(\mathbf{x})^2] = -\beta \frac{d\ \ln a}{d\beta}\sigma\ . \qquad (18)$$

The comparison shown in the Table IV gives a somewhat larger value for the ratio σ_A/σ. Nevertheless, it is still compatible with the uncertainty of the current estimates for the β function, $-\beta d\ \ln a/d\beta = 7.7 \pm 1.0$.

It is apparent from Eq. (17) that the self-energy contribution to the total action is not enhanced by the

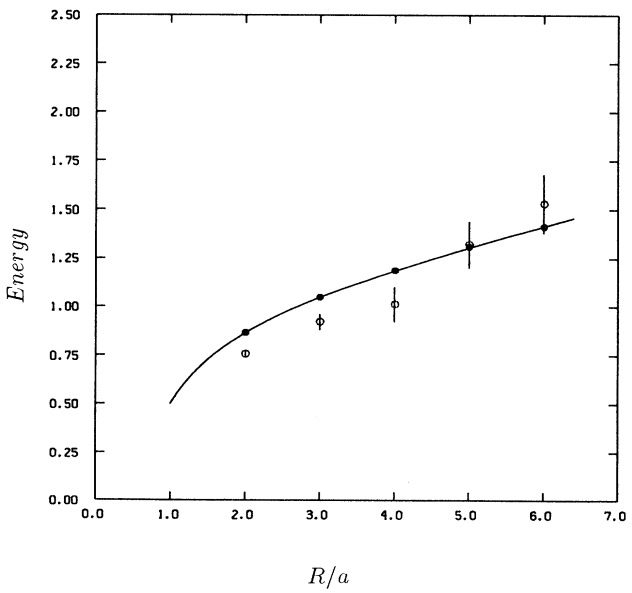

FIG. 6. Energy sum rule. Open circles show the integrated density; solid circles show the potential plus the self-energy. Solid line corresponds to the fit [Eq. (14)]; $\beta = 2.4$.

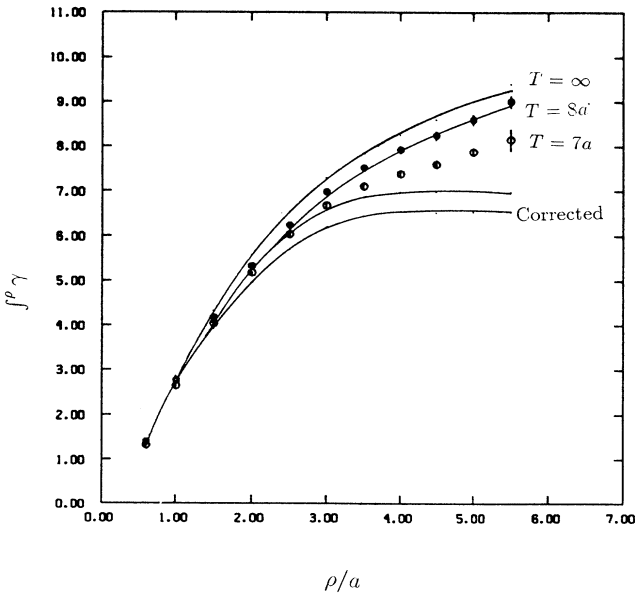

FIG. 7. Integrated, up to ρ, transverse profiles of the action density (GeV). Open circles show $T=7a$ and solid circles show $T=8a$ data. Upper band represents the extrapolated to $T=\infty$ cumulants and the uncertainty of the fit. Lower band gives values corrected for the nonzero background. $\beta = 2.4$.

TABLE IV. Energy and the action, in GeV/fm, stored in the transverse middle slice and normalized to the unit length of the tube.

R/a	T/a	6	7	8	∞
5	Energy	0.68(06)	0.94(11)	0.86(17)	0.72(07)
	Condensate	7.37(08)	7.55(11)	8.12(17)	7.88(10)
6	Energy	0.76(12)	0.68(20)		0.82(17)
	Condensate	7.40(10)	8.12(20)	9.6(1.7)	8.34(20)

$-\beta d\ln a/d\beta$ factor. It remains approximately at the same absolute level[5,7] and is given by the last term in Eq. (17). This effect can be seen more directly in our data. Figure 8 shows the longitudinal profile of the energy/action density. Indeed, the energy profile is more peaked around the sources than that of the condensate. More quantitatively, the height of the peaks about the approximately flat, confining background, is the same, while the ratio of the action and the energy densities, at the plateau, is roughly given by $-\beta d\ln a/d\beta$. For the distributions extrapolated in T, agreement is even better. On the other hand, the absolute values of the self-energy, as extracted from the potential fits, seem rather large compared to the energy stored in the direct vicinity of the sources. The large self-energy part has a dramatic effect on the global action sum rule. It turns out that after subtracting c/a from $E_0(R)$, the RHS of Eq. (17) is much too small to account for the sum of our action density. Since our "experimental uncertainties" are much smaller for the action than for the energy, we feel that the action sum rule is the good place to determine independently the β function, the self-energy, and the self-action entering Eq. (17). To this end we have fitted our data for $A(R)$ with the formula (17), treating $\xi\equiv-\beta d\ln a/d\beta$ and $z\equiv-\xi E_{\rm self}+A_{\rm self}$ ($E_{\rm self}\equiv c/a$ and $A_{\rm self}\equiv-\beta\dot{c}/a$) as free parameters, and taking $E_0(R)$ from the potential fits. The results are shown in Fig. 9 and Table V. The best value for ξ agrees very well with the one quoted in Ref. 4 and has much smaller errors. However, the only independent combination of the self-energy and self-action, namely, z, is smaller almost by the factor of 2. This is exactly the effect we have mentioned earlier. With the value quoted by Sommer or Michael (0.87 GeV) for $E_{\rm self}$ and $A_{\rm self}=0.51$ GeV (as read from Fig. 4 of Ref. 4), the action sum rule is inconsistent.

A possible explanation of this discrepancy is the operational definition of the self-energy adapted in Refs. 4 and 10. To account for the lattice artifacts in fitting the potential, one has to use the lattice propagator instead of the Coulomb one. On the other hand, derivation of the sum rule[5] requires splitting of the $q\bar{q}$ energy into scaling physical potential and the remainder defined as the self-energy.

An alternative explanation is that our semiclassical definition of the energy momentum tensor is too simplified; cf. Eqs. (3)–(5). This form was being used in all simulations mainly because of the low precision of the available Monte Carlo data. It is conceivable that for the

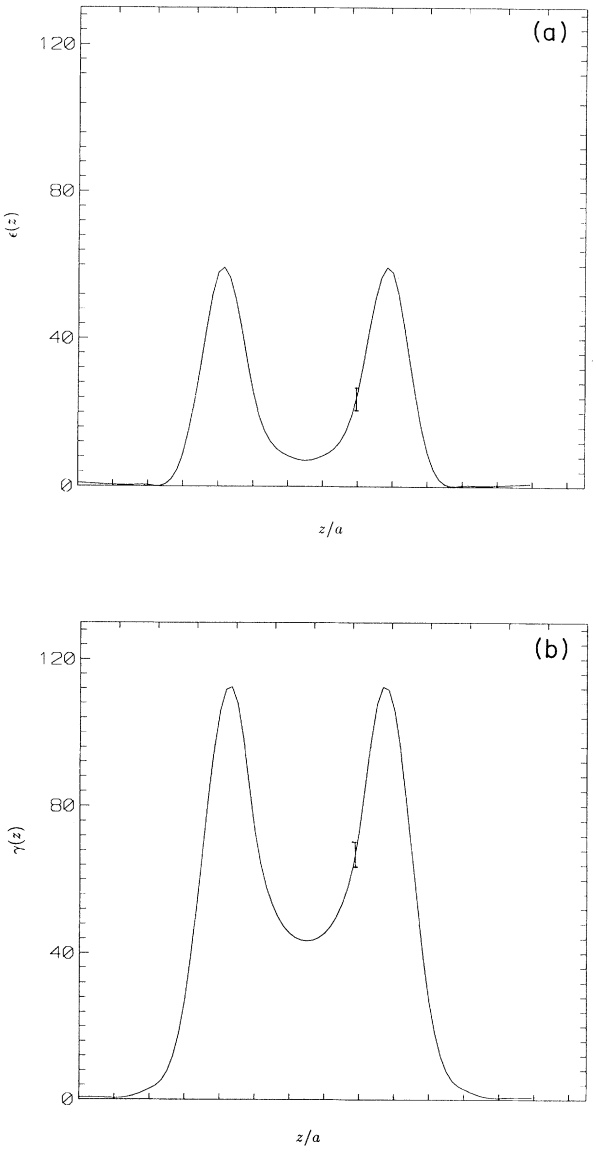

FIG. 8. Longitudinal profiles of the (a) energy and (b) action densities, in GeV/fm^3, at $x_\perp=0$. Typical error is also shown. $R=5a$, $T=7a$, and $\beta=2.4$.

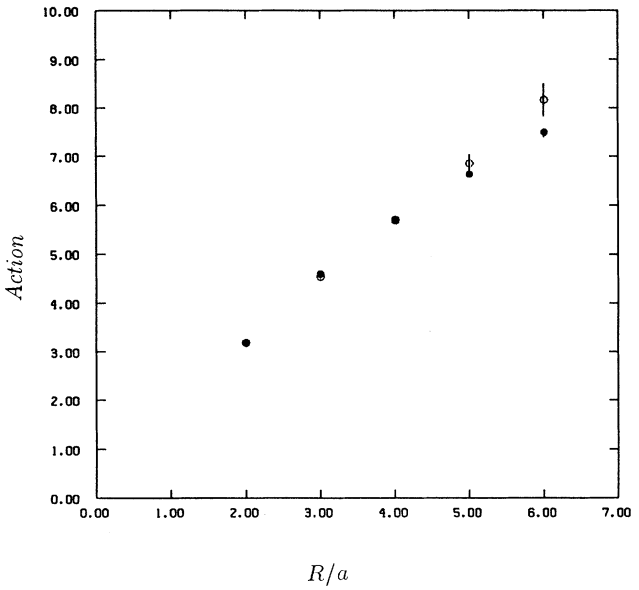

FIG. 9. Action sum rule. Open circles show integrated action density; solid circles represent the RHS of Eq. (17) as described in the text; $\beta=2.4$.

first time we have achieved the accuracy which allows one to distinguish between the semiclassical and full quantum definitions which was recently proposed.[34–36] We are looking forward to studying this problem in detail.

V. SUMMARY AND CONCLUSIONS

We attempt rather extensive Monte Carlo study of the distribution of the chromoelectric field around the static $q\bar{q}$ pair. In this article we discuss the global quantities, i.e., the potential and sum rules involving fully integrated space distributions. In the companion paper[28] we will concentrate on the local properties of the distributions. Many tests performed on simpler observables (Wilson loops and $q\bar{q}$ potential itself) have shown consistency of our data with the results of other authors.[4,10,33]

Compared with the last[25,26] year, we have improved measurements of the fields in the close vicinity of the sources. This allows for direct tests of the lattice action sum rules, which were derived some time ago.[5]

The energy sum rule does not have any free parameters. The three-dimensional (3D) integral of the independently measured energy density should be equal to the total energy of the static $q\bar{q}$ system. For larger $q\bar{q}$ distances $R=4a-6a$, the sum rule is very well satisfied. For small R the summed energy is systematically smaller ($\sim 10\%$) than the total energy of the $q\bar{q}$ state. The discrepancy is statistically significant and is bigger than the systematic uncertainties of our procedure. We think it is caused by the a/R effects, i.e., too coarse a lattice for an adequate description of the small tubes.

TABLE V. Results of fitting the action sum rule.

$\xi=-\beta\frac{d\ln a}{d\beta}$	$z=-\xi E_{\rm self}+A_{\rm self}$
7.76(11)	−3.45(9) GeV

The action sum rule relates the space integral of the gluon condensate to the scaling part of the $q\bar{q}$ energy. Since both observables can be measured quite accurately, this relation allows for very precise determination of the SU(2) β function and the quark self-energy. It turns out that, for the optimal choice of these parameters, the sum rule is well saturated for all available values of R/a. The value of the β function, obtained in this way, is in good agreement with the one measured independently by other authors who used different approaches. However, the quark self-energy is significantly lower than the one obtained from the potential fits. In our opinion this is caused by the two, not necessarily equivalent, definitions of the self-energy used in the literature.

Recently, Caracciolo *et al.* in a series of very interesting papers have presented and discussed the full quantum definition of the energy-momentum tensor on the lattice[34–36] (see also Ref. 37). The accuracy of our data, especially for the gluon condensate, offers a possibility to distinguish it from the simple semiclassical definition used until now. It is possible that the small deviations we are observing can be accounted for by this difference. This subject requires further study, especially adapting their approach to the $q\bar{q}$ sector of the Hilbert space.

ACKNOWLEDGMENTS

We wish to thank our collaborator on the companion paper of this one, Vandana Singh, for helping in the handling of a large amount of data for this work also. This work was supported in part by the U. S. Department of Energy under Contract No. DE-AS05-77ER05490 and by the Polish Government under Grants Nos. CPBP 01.03 and CPBP 01.09.

[1]M. Fukugita and T. Niuya, Phys. Lett. **132B**, 374 (1983).
[2]J. W. Flower and S. W. Otto, Phys. Lett. **160B**, 128 (1985).
[3]R. Sommer, Nucl. Phys. **B291**, 673 (1987).
[4]R. Sommer, Nucl. Phys. **B306**, 180 (1988).
[5]C. Michael, Nucl. Phys. **B280** [FS18], 13 (1987).
[6]A. Huntley and C. Michael, Nucl. Phys. **B286**, 211 (1987).
[7]I. H. Jorysz and C. Michael, Nucl. Phys. **B302**, 448 (1987).
[8]C. Michael and M. Teper, Nucl. Phys. **B305**, 453 (1988).
[9]N. A. Campbell, A. Huntley, and C. Michael, Nucl. Phys. **B206**, 51 (1988).
[10]S. Perantonis, A. Huntley, and C. Michael, Nucl. Phys. **B326**, 544 (1989); see also S. Perantonis, in *Lattice '88*, proceedings of the International Symposium, Batavia, Illinois, 1988, edited by A. S. Kronfeld and P. B. MacKenzie [Nucl. Phys. B (Proc. Suppl.) **9**, 249 (1989)].
[11]W. Feilmair, M. Faber, and H. Markum, Phys. Rev. D **39**, 1409 (1989).
[12]G. Eder, M. Faber, W. Feilmair, and H. Markum, in *Lattice*

'88 (Ref. 10), p. 394.
[13]M. Muller, M. Fabor, W. Feilmair, and H. Markum, Nucl. Phys. **B335**, 502 (1990).
[14]Ph. de Forcrand, V. Linke, and I. O. Stamatescu, Nucl. Phys. **B304**, 645 (1988).
[15]D. G. Caldi and T. Sterling, Phys. Rev. Lett. **60**, 2454 (1988); Phys. Rev. D **40**, 3447 (1989).
[16]M. Campostrini, A. De Giacomo, M. Maggiore, H. Panagopoulos, and E. Vicari, Phys. Lett. B **225**, 403 (1989).
[17]A. Duncan and R. Mawhinney, Phys. Lett. B **241**, 403 (1990).
[18]H. B. Nielsen and P. Olesen, Nucl. Phys. **B61**, 45 (1973).
[19]M. Lüscher, Nucl. Phys. **B180** [FS2], 317 (1981).
[20]M. Lüscher, G. Münster, and P. Weisz, Nucl. Phys. **B180** [FS2], 1 (1981).
[21]M. Baker, J. S. Ball, and F. Zachariasen, Phys. Rev. D **41**, 2612 (1990).
[22]E. Bagan, Phys. Lett. B **248**, 353 (1990).
[23]J. Wosiek and R. Haymaker, Phys. Rev. D **36**, 3297 (1987).
[24]J. Wosiek, in *Field Theory on the Lattice,* proceedings of the International Symposium, Seillac, France, 1987, edited by A. Billoire *et al.* [Nucl. Phys. B (Proc. Suppl.) **4**, 52 (1988)].
[25]R. W. Haymaker and J. Wosiek, Acta Phys. Pol. B **21**, 403 (1990).
[26]R. W. Haymaker, Y. Peng, V. Singh, and J. Wosiek, in *Lattice '89,* proceedings of the International Symposium, Capri, Italy, 1989, edited by R. Petronzio *et al.* [Nucl. Phys. B (Proc. Suppl.) **17**, 558 (1990)].
[27]R. W. Haymaker, Y. Peng, V. Singh and J. Wosiek, in *Proceedings of the Annual Meeting of the Division of Particles and Fields of the APS,* Houston, Texas, 1990 (World Scientific, Singapore, 1990), p. 789.
[28]R. W. Haymaker, V. Singh, and J. Wosiek (unpublished).
[29]M. Creutz, Phys. Rev. D **36**, 515 (1987).
[30]G. Parisi, R. Petronzio, and F. Rapuano, Phys. Lett. **128B**, 418 (1983).
[31]B. Bunk (unpublished).
[32]H.-Q. Ding, Phys. Lett. B **200**, 133 (1988).
[33]F. Gutbrod, Z. Phys. C **30**, 585 (1986).
[34]S. Caracciolo, G. Curci, P. Menotti, and A. Pelissetto, Nucl. Phys. **B309**, 612 (1988).
[35]S. Caracciolo, G. Curci, P. Menotti, and A. Pelissetto, Ann. Phys. (N.Y.) **197**, 119 (1990).
[36]S. Caracciolo, G. Curci, P. Menotti, and A. Pelissetto, Phys. Lett. B **228**, 375 (1989).
[37]M. Campostrini, G. Curci, A. Di Giacomo, and G. Paffuti, Z. Phys. C **32**, 377 (1986).